Environmental Pollution 293 (2022) 118521

Contents lists available at ScienceDirect

Environmental Pollution

journal homepage: www.elsevier.com/locate/envpol

Removal of phosphate from water by paper mill sludge biochar☆

Ming Zhang [a], Kun Lin [a], Xiaodian Li [a], Lijun Wu [b], Jie Yu [a], Shuang Cao [a], Dong Zhang [c], Liheng Xu [a], Sanjai J. Parikh [d], Yong Sik Ok [e,*]

[a] Department of Environmental Engineering, China Jiliang University, Hangzhou 310018, Zhejiang Province, China
[b] China Huadong Engineering Corporation Limited, Hangzhou 311122, Zhejiang Province, China
[c] Institute of Environmental Materials & Technology, Hangzhou Dianzi University, Hangzhou 310018, Zhejiang Province, China
[d] Department of Land, Air and Water Resources, University of California – Davis, Davis, CA, USA
[e] Korea Biochar Research Center, APRU Sustainable Waste Management Program & Division of Environmental Science and Ecological Engineering, Korea University, Seoul, Republic of Korea

ARTICLE INFO

Keywords:
Phosphate
Biochar
Adsorption
Paper mill sludge
Zero-valent iron (ZVI)
One-step process
Waste-to-wealth strategy

ABSTRACT

Biochar modification by metals and metal oxides is considered a practical approach for enhancing the adsorption capacity of anionic compounds such as phosphate (P). This study obtained paper mill sludge (PMS) biochar (PMSB) via a one-step process by pyrolyzing PMS waste containing ferric salt to remove anionic P from water. The ferric salt in the sludge was transformed into ferric oxide and zero-valent-iron (Fe^0) in N_2 atmosphere at pyrolysis temperatures ranging from 300 to 800 °C. The maximum adsorption (Q_m) of the PMSBs for P ranged from 9.75 to 25.19 mg P/g. Adsorption is a spontaneous and endothermic process, which implies chemisorption. PMSB obtained at 800 °C (PMSB800) exhibited the best performance for P removal. Fe^0 in PMSB800 plays a vital role in P removal via adsorption and coprecipitation, such as forming the ≡Fe–O–P ternary complex. Furthermore, the possible chemical precipitation of P by CaO decomposed from calcite ($CaCO_3$; an additive of paper production that remains in PMS) may also contribute to the removal of P by PMSB800. Moreover, PMSBs can be easily separated magnetically from water after application and adsorption. This study achieved a waste-to-wealth strategy by turning waste PMS into a metal/metal oxide-embedded biochar with excellent P removal capability and simple magnetic separation properties via a one-step pyrolysis process.

1. Introduction

Phosphorus (P) is an essential element in all living organisms because of its importance in forming genetic materials, biological membranes, and energy-converting carriers (Marschner and Marschner, 2012). However, the large-scale disturbance of P cycles in the environment caused by anthropogenic activity has led to the accumulation of P in the aquatic environment, causing eutrophication and threatening the health of ecosystems and human safety (Conley et al., 2009; Xia et al., 2020). P is also considered the primary limiting nutrient for hydrophytes (Schindler, 1974). Thus, P reduction/control can inhibit eutrophication in lakes (Conley et al., 2009). In conventional wastewater treatment processes, biological methods, such as aerobic/oxic (A/O) processing by P-accumulating organisms (Oehmen et al., 2007), are commonly adopted, and these organisms can store and release P in response to the periodic alternation of environmental conditions (Nielsen et al., 2019). In addition, the precipitation of P by metal or metal oxides is considered a supplementary method for P removal (Ye et al., 2017).

The adsorption of P from water by biochar, a solid residue obtained from biomass pyrolysis, has been widely investigated over the past decade (Cui et al., 2016; Fang et al., 2014; Gong et al., 2017b; Jung et al., 2015). The surfaces and pores of biochar formed during biomass pyrolysis and the abundant functional groups on biochar are able to facilitate good adsorption performance (Ahmad et al., 2014). However, according to previously reported studies, the capability of unmodified biochars for P removal has varied greatly, with maximum P adsorption ranging from 1.37 to 193 mg P/g (Zhang et al., 2020a). Some biochars have a very weak affinity for P, which may be caused by the electrostatic repulsion between the negatively charged biochar surface and the anionic forms of P (Jung et al., 2015). Certain biochars may even release P into water rather than adsorb it (Cui et al., 2016). However, biochars with a high-P adsorption capacity have been observed (Fang et al.,

☆ This paper has been recommended for acceptance by Baoshan Xing.
* Corresponding author.
E-mail address: yongsikok@korea.ac.kr (Y.S. Ok).

https://doi.org/10.1016/j.envpol.2021.118521
Received 3 August 2021; Received in revised form 8 November 2021; Accepted 13 November 2021
Available online 15 November 2021

2014). The mineral elements in both ionic and oxide forms could potentially play an indispensable role in the adsorption and removal of P from water (Yin et al., 2018). Zeng et al. (2013b) evaluated the P removal capacities of biochars obtained from phytoremediation plants and found that plant-derived biochar with higher magnesium (Mg) content has a higher P removal efficiency. Similarly, Yao et al. (2013b) observed that biochar pyrolyzed from Mg-enriched tomato leaves adsorbed a much higher amount of P. Jung et al. (2015) found that biochars with higher Ca/P or Mg/P ratios can have higher P adsorption capabilities because the divalent cation bridging effect is believed to be responsible for binding P on biochar. These findings led to a method for improving the P removal performance of biochar by modifying it with metals or metal oxides. For instance, MgO-modified biochar obtained by the pyrolysis of $MgCl_2$ immersed in sugar beet tailing was found to have a much higher adsorption capacity for P (835 mg P/g) (Zhang et al., 2012). Biochar modification with Mg and poly diallyl dimethyl ammonium chloride (pDADMAC), resulted in ~100 times increase in P sorption (70.5–97.1 mg P/g for Mg-doped and pDADMAC biochars) compared to unmodified softwood and maple biochars (Wang et al., 2020). The maximum adsorption capacity of sawdust biochar for P increased from 10.67 to 47.57 mg P/g after modification by lanthanum (La) (Wang et al., 2015). Al-doped biochars obtained from poultry manure and sugarcane straw also have extremely high P adsorption capacities of 702 and 759 mg P/g, respectively (Novais et al., 2018a).

However, modification processes for biochar are costly, time-consuming, and potentially harmful to the environment due to the use of large quantities of chemicals. To circumvent these drawbacks, we hypothesized that biochar with high P adsorption capacity could be obtained via a one-step process based on the pyrolysis of waste biomass with high metal/metal oxide content, omitting the need for additional modification. In this study, paper mill sludge (PMS) containing iron ions (from flocculants used in paper mill wastewater treatment) and $CaCO_3$ (from additives used in paper production) was used as a feedstock to produce biochar via a one-step process. The objectives of this study were to 1) characterize the properties of PMS biochars, 2) evaluate adsorption capacities for P removal, and 3) reveal the possible mechanisms for P removal. The results obtained from this study may provide insight into the cost-effective use of industrial waste for pollution control.

2. Material and methods

2.1. Preparation of biochars derived from paper mill sludge

In this study, PMS was obtained from the wastewater treatment plant of a paper production company in South Korea and used as a biochar feedstock. The PMS contained a significant amount of $CaCO_3$ from the additives used in paper production and iron ions from the coagulant used during wastewater treatment. Ca (7.93%) and Fe (17.69%) content in the PMS at dry weight was determined by an Inductively Coupled Plasma Optical Emission Spectroscopy (ICP-OES, Agilent 720 ES) after acid digestion. The PMS was washed with tap water to remove dust and possible dissolved substances and then dried in an oven at 100 °C for 24 h. The dried PMS was crushed using a triturator and stored for further use. The PMS powder was then placed in a crucible and pyrolyzed in a temperature-controlled muffle furnace equipped with a quartz cup reactor. The crucible was kept in a capped quartz cup throughout the entire pyrolysis process, and the quartz cup was filled with continuous gentle purging of N_2 to create an O_2-free environment. The heating rate was 10 °C/min, and the peak temperatures for the PMS biochars were 300 °C, 500 °C, 700 °C, and 800 °C, which was maintained for 1 h and then the biochars were cooled to room temperature in the furnace. The PMSBs obtained at these temperatures are denoted as PMSB300, PMSB500, PMSB700, and PMSB800, respectively.

2.2. Batch adsorption studies

Potassium dihydrogen phosphate (KH_2PO_4) was used to prepare the P solution. A stock solution of 500 mg P/L KH_2PO_4 was prepared, and dilutions were prepared using distilled water. The exact concentrations of P in the test and control samples were determined after batch adsorption using the Chinese national environmental standard method (water quality-determination of total phosphorus-ammonium molybdate spectrophotometric method, GB 11893–89).

Batch adsorption experiments were conducted by mixing different amounts of PMSBs (0.03 g, 0.04 g, 0.03 g, and 0.01 g for PMSB300, PMSB500, PMSB700, and PMSB800, respectively) with 20 mL of P solution in 22-mL glass tubes with Teflon-lined caps. The pH of the solution was not further adjusted. For adsorption kinetics, the initial concentration of P was maintained at 20 mg P/L, and the mixtures of PMSB and P solution were shaken for 0.25, 0.5, 1, 2, 3, 4, 6, 8, 12, 16, 20, 24, and 36 h at the temperature of 25 ± 0.5 °C at a speed of 150 rpm in a shaker incubator. The final solution was filtered using 0.22-μm hydrophilic syringe filters, and the P concentrations in the leachate were analyzed. The P concentration differences between the samples with PMSBs and control samples without PMSBs were calculated to determine the amount of P adsorbed. To quantitatively compare the adsorption kinetics using different PMSBs, a pseudo-first-order (PFO) kinetic model (Lagergren, 1898) and pseudo-second-order (PSO) kinetic model (Ho, 1995; Ho and McKay, 1999) were employed, as described in Eqs. (1) and (2), respectively:

$$Q_t = Q_{e1}\left(1 - e^{-k_1 t}\right) \tag{1}$$

$$Q_t = \frac{k_2 Q_{e2}^2 t}{1 + k_2 Q_{e2} t} \tag{2}$$

where, Q_t is the adsorption amount of P (mg P/g) on PMSBs at time t. Q_{e1} and Q_{e2} are the maximum adsorption amount estimated by the first and second-order kinetic models, respectively. k_1 and k_2 are the kinetic rate constants of the first and second-order kinetic models, respectively.

For adsorption isotherms, the same amount of PMSB as in the kinetic experiments was used. P solutions at various concentrations (0, 4, 8, 12, 16, 20, 24, 28, 32, 36, and 40 mg P/L) were mixed with the PMSBs in 22-mL glass tubes with Teflon-lined caps. All tubes were shaken at a temperature of 25 ± 0.5 °C at a speed of 150 rpm in a shaker incubator for 24 h. To describe the isotherm patterns of the PMSBs for P, the Langmuir adsorption model (Langmuir, 1918) and Freundlich adsorption model (Freundlich, 1906) were employed, as shown in Eqs. (3) and (4), respectively:

$$Q_e = \frac{Q_m K_L C_e}{1 + K_L C_e} \tag{3}$$

$$Q_e = k_F C_e^{1/n} \tag{4}$$

where Q_e is the equilibrium adsorption amount of P (mg P/g) at an aqueous equilibrium concentration of C_e (mg P/L), and Q_m is the maximum adsorption amount of P (mg P/g) estimated by the Langmuir adsorption model. K_L and K_F are constants of the Langmuir and Freundlich model, respectively. $1/n$ represents the degree of nonlinearity of the adsorption isotherm.

To determine the influence of temperature on the adsorption of P by PMSB, PMSB800 was selected as the representative case due to its superior performance. The adsorption isotherms were carried out as described earlier at temperatures of 5 °C, 15 °C, and 25 °C.

2.3. Characterization of paper mill sludge biochars

The morphologies of the PMSBs were observed using scanning electron microscopy (SEM, Hitachi SU8200, Japan) and transmission electron microscopy (TEM) with an energy dispersive spectrometer

(TEM-EDS, FEI Tecnai G2 F20, Netherlands). The surface area and pore volume of the PMSBs were analyzed using the N_2 adsorption-desorption method using a surface area analyzer (Gemini 2390, USA). The X-ray diffraction (XRD) patterns of the samples were obtained using an XRD diffractometer (Bruker D8 Advance, Germany) at a working voltage and current of 40 kV and 40 mA, respectively, at a scanning speed of 5°/min in the range of 5°–90°. The X-ray photoelectron spectroscopy (XPS) was obtained from an electron spectrometer (ESCALab220i-XL, VG Scientific, UK).

3. Results and discussion

3.1. Adsorption kinetics and isotherms

3.1.1. Adsorption kinetics

The kinetics of P adsorption by PMSBs are shown in Fig. 1. The adsorption amounts increased quickly in the first stage of adsorption due to the maximum concentration differences between the surface of the adsorbent (approximately 0) and the solution (initial concentration), which provided the greatest force for adsorption. With further increases in adsorption time, the adsorption amount increased slowly, and the kinetic curves gradually reached equilibrium. As shown in Fig. 1, the equilibrium times of PMSB300, PMSB500, and PMSB700 were less than 4 h. However, PMSB800 took significantly longer (approximately 24 h) to reach equilibrium.

A PFO and PSO kinetic model were employed in this study to describe the kinetic curves quantitatively, and the fitted parameters are listed in Table S1. Both models fit the kinetic data well, with correlation coefficients (R^2) greater than 0.87. However, the PSO kinetic model performed better, with a significantly higher R^2, indicating that chemical adsorption occurred during the adsorption of P by PMSBs (Ho, 1995; Ho and McKay, 1999). At the same initial concentration of P (20 mg P/L), PMSB800 exhibited a significantly higher adsorption amount, despite having the lowest adsorption rate constants (shown as k_1 and k_2 in Table S1).

3.1.2. Adsorption isotherms

The adsorption isotherms of P by PMSBs are shown in Fig. 2. All isotherms were significantly nonlinear, indicating surface-based adsorption. The Langmuir and Freundlich adsorption models were employed in this study, and the fitting parameters of these two models for the adsorption of P by PMSBs are provided in Table S2. The results demonstrate that PMSB800 had the highest adsorption capacity (25.19 mg P/g), followed by PMSB700, PMSB 500, and PMSB300. Although the adsorption capacity of PMSB700 was slightly higher than PMSB500 and PMSB300 in the tested concentration range, the Langmuir model-estimated Q_m values of PMSB700, PMSB500, and PMSB300 were all similar (9.75–11.44 mg P/g). Many biochars have a poor capacity for P removal from water (Cui et al., 2016; Gong et al., 2017a; Jung et al., 2015) as the surfaces of biochars are generally negatively charged (Ahmad et al., 2014), which may lead to strong electrostatic repulsion between the biochar and the P anions, inhibiting the adsorption of P. In addition, biochar contains inherent P, which may be released in water (Hale et al., 2013; Park et al., 2015). As a result, the Q_m of PMSB800 in this study was higher than most of the previously reported values for pristine biochar (Chandra et al., 2020; Zeng et al., 2013a; Zhou et al., 2019). The possible reasons are discussed in Section 3.2. However, there have been a few high Q_m values reported previously, some exceeding 100 mg P/g (Fang et al., 2014; Gong et al., 2017a; Novais et al., 2018b).

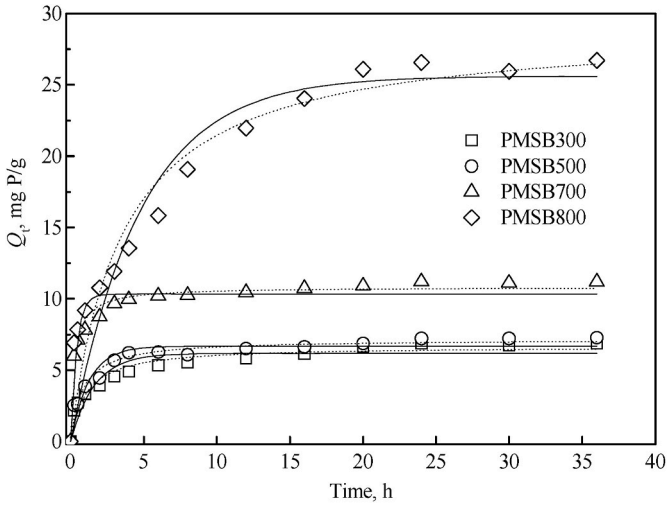

Fig. 1. Adsorption kinetics of P adsorbed by PMSBs. The solid line is the PFO kinetic model-fitted curve, and the dotted line is the PSO kinetic model-fitted curve.

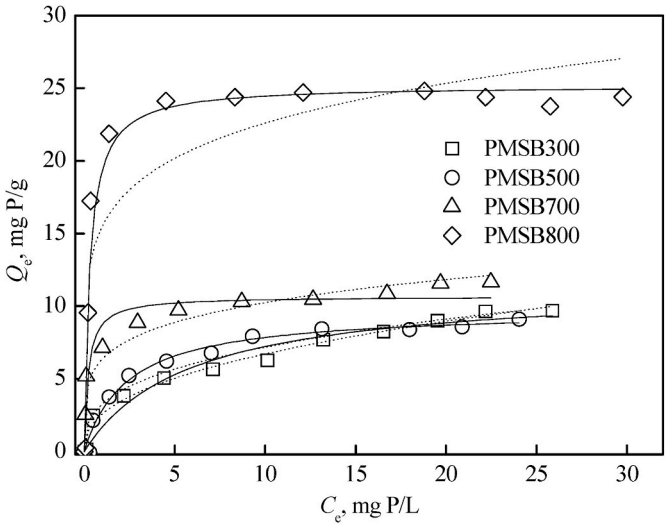

Fig. 2. Adsorption isotherms of P by PMSBs. Solid lines represent the Langmuir adsorption model-fitted curves, while the dotted lines represent the Freundlich adsorption model-fitted curves.

The enhanced adsorption capacity of biochar with increasing pyrolysis temperature is generally associated with the increase in surface area (Chintala et al., 2013; Zeng et al., 2013a). Although the surface areas of PMSBs increased from 37.88 to 95.16 m^2/g with an increase in pyrolysis temperature from 300 °C to 800 °C (Table S3), the increase in adsorption capacities was not linear. In particular, an increase in the surface areas of PMSBs pyrolyzed from 300 °C to 700 °C led to no significant change in P adsorption amounts, as Q_m values ranged from 9.75 to 11.44 mg P/g. Other mechanisms are dominantly involved in the enhancement of P adsorption. Further characterization of the PMSBs was conducted to reveal other potential mechanisms, which are discussed in Section 3.2.

3.1.3. Effect of ambient temperature on P adsorption by paper mill sludge biochars

To investigate the influence of ambient temperature on P adsorption by PMSBs, PMSB800 was selected as a representative adsorbent owing to its superior performance for P adsorption. The adsorption isotherms at different temperatures are shown in Fig. 3. All isotherms were fitted using the Langmuir adsorption model, and the corresponding parameters are listed in Table 1. The results revealed significant differences among the isotherms from 5 °C to 25 °C, with the increase in ambient temperature enhancing the Q_m of PMSB800 markedly from 6.89 to 25.19 mg P/g, indicating an endothermic adsorption process.

Similar trends were found in investigations of P adsorption by corn biochar at 25 °C–45 °C (Fang et al., 2014) and of peanut shell biochar at

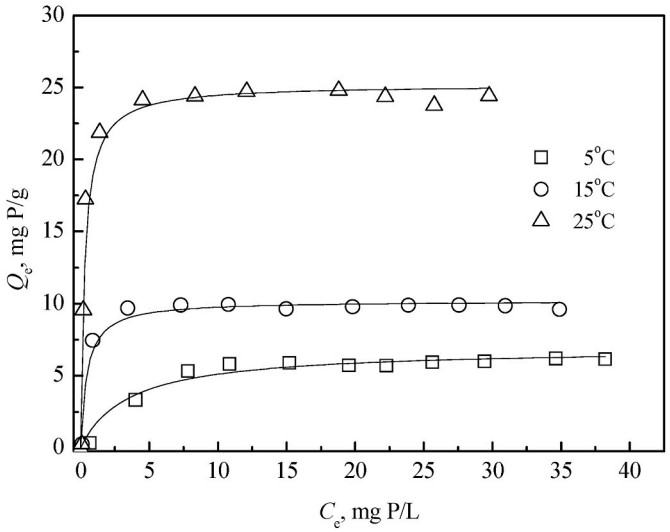

Fig. 3. Effect of temperature on the adsorption of P by PMSB800.

Table 1
Thermodynamic parameters of the adsorption of P by PMSB800 at different temperatures.

T, K	K, $\times 10^6$ L/kg	Q_m, mg P/g	R^2	ΔH, kJ/mol	ΔS, kJ/mol·K	ΔG, kJ/mol
278	0.284	6.89	0.9711	85.33	0.413	−29.484
288	2.180	10.20	0.9732			−33.614
298	3.324	25.19	0.9572			−37.744

10 °C–30 °C (Jung et al., 2015). The random thermal motion of ions may be enhanced by an increase in temperature, leading to a higher possibility of collisions between P ions and the biochar surface (Kilic et al., 2013; Wang et al., 2016).

To further illustrate the influence of temperature on the adsorption of P by PMSB800, thermodynamic analysis was employed. Thermodynamic parameters (Table 1) were obtained using the Van't Hoff equation (Zhang et al., 2014; Zhu and Zhu, 2008), which can be described as:

$$lnK = -\frac{\Delta H}{RT} + \frac{\Delta S}{R}$$

where K is the fitted adsorption coefficient of the Langmuir adsorption model, R is the ideal gas constant (8.314 $\times 10^{-3}$ kJ/mol·K), and T is the temperature (K). ΔH and ΔS are the enthalpy and entropy changes in the adsorption process, respectively, and the Gibbs free energy change (ΔG) can be calculated as follows:

$$\Delta G = \Delta H - T\Delta S$$

The positive ΔH value indicates that P adsorption on PMSB800 is an endothermic process, meaning an increase in ambient temperature can promote P adsorption. ΔG was negative at all temperatures, implying that the adsorption was spontaneous. In addition, the ΔG values decreased with increased temperature, indicating that higher temperatures are favorable for the adsorption of P on PMSB800 (Zhang et al., 2014; Zhou et al., 2019; Zhu and Zhu, 2008).

3.2. Characterization of paper mill sludge biochars

3.2.1. Scanning electron microscopy and transmission electron microscopy observation

The morphologies of the PMSBs were observed using SEM and TEM (Fig. 4). There was no significant pore structure in the PMSBs, which is in accordance with their low Brunauer–Emmett–Teller (BET) surface areas (37.88–95.16 m^2/g). With an increase in pyrolysis temperature, crystal-like nanoparticle aggregates were found in PMSB500, PMSB700, and PMSB800. Yoon et al. (2017) explained that mineral aggregates formed after pyrolysis might block the pores in the biochar matrix. Thus, there was no significant increase in the number of micropores or mesopores with an increase in pyrolysis temperature. Similarly, Ruan et al. (2015) reported that a bentonite/hematite-embedded biochar has a small BET surface area.

To further determine the structure and composition of the PMSBs, elemental mapping of PMSB800 by TEM-EDS was employed to identify its elemental composition and especially to account for the formed crystal-like aggregates. The results are shown in Fig. 5. The main elements in PMBS800 were Fe, Ca, C, and O. There was a higher density of Fe and O content in the crystal-like aggregates, indicating that the crystals might be Fe or Fe oxides. The Fe in the PMSBs was added as ferric salts during the paper mill wastewater treatment as a coagulant. The pyrolysis of PMS into PMSB in the N_2 atmosphere provided a reducing atmosphere, and Fe ions were transformed into iron oxides (FeO_x) or zero-valent-iron (ZVI, Fe^0). Fe salts or Fe minerals, such as Fe^{3+}, Fe^{2+}, $FeCO_3$, and Fe-rich red mud, have frequently been used as modification agents to produce metallic modified biochar to improve magnetic properties or contaminant adsorption capability (Cho et al., 2019; Yoon et al., 2020; Yoon et al., 2017; Yoon et al., 2019a; Zhang et al., 2015). Thus, there is no modification process needed for the metal-enriched biochar produced via a one-step pyrolysis process in this study. It has been reported that the Mg/MgO coated biochar can significantly enhance the adsorption of P, and they speculated that higher point-of-zero-charges of $Mg(OH)_2$/MgO (about 12) might cause positively charged biochar surface (Yao et al., 2013a). Therefore, the

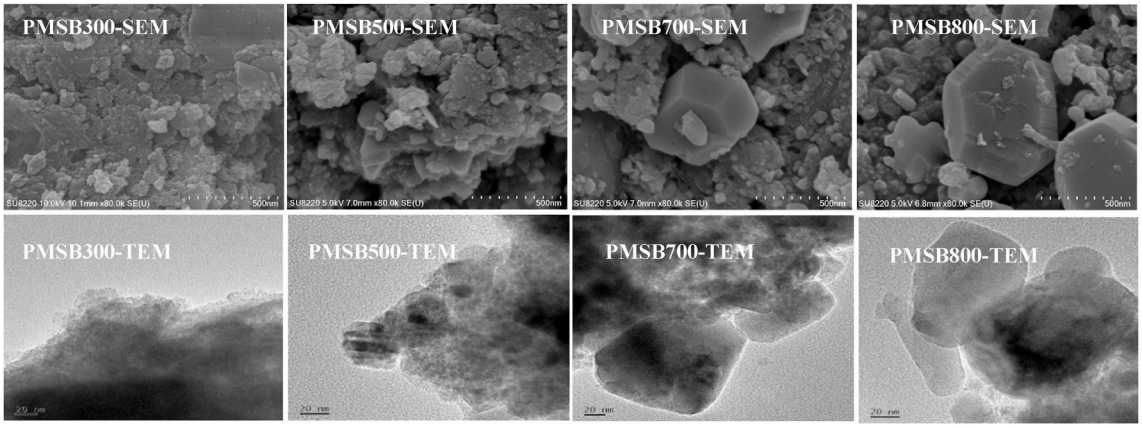

Fig. 4. SEM and TEM images of PMSB300, PMSB500, PMSB700, and PMSB800.

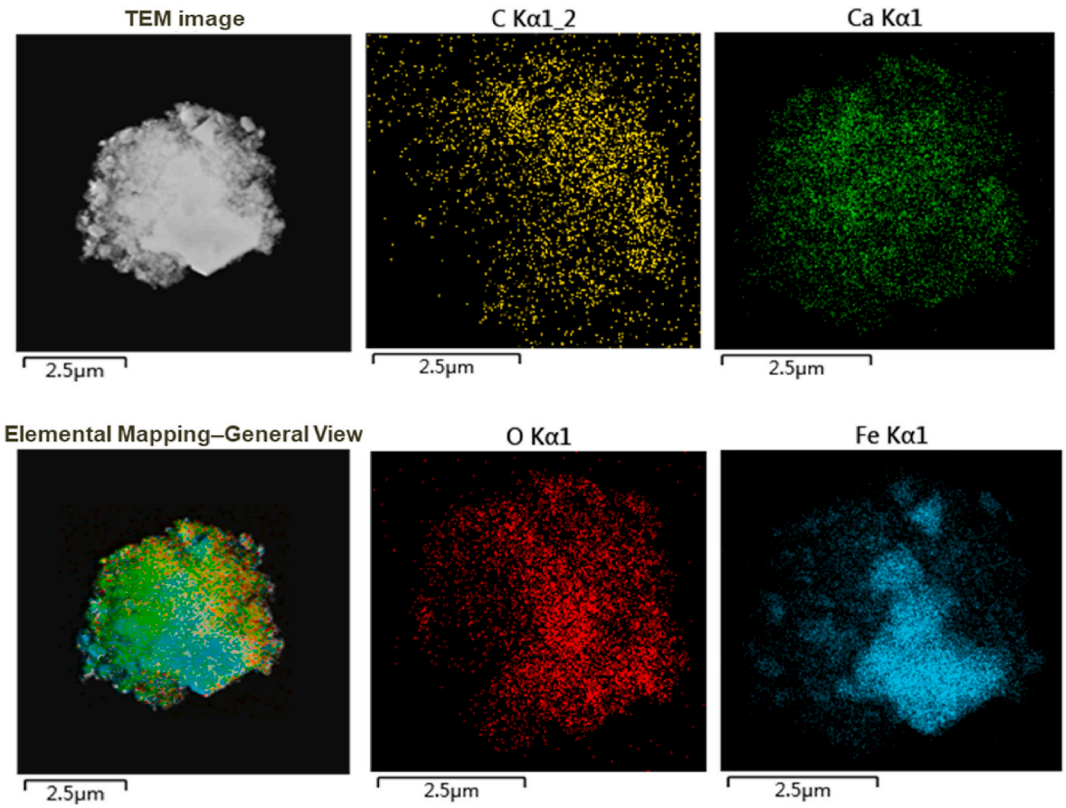

Fig. 5. Elemental mapping of PMSB800 by TEM-EDS.

FeO_x- or Fe^0-coated PMSB may hinder the negative charges on the biochar surface, reducing electrostatic repulsion and increasing the P adsorption capacity of the PMSBs.

3.2.2. *X-ray diffraction patterns of paper mill sludge biochars*

The XRD patterns of the PMSBs were scanned in the 2θ range of 20°–70° (Fig. 6). Peaks typically assigned to $CaCO_3$ were found in the XRD patterns of PMSB300, PMSB500, and PMSB700 at 2θ = 29.4°, 47.1°, and 48.5° (PDF#47–1743), respectively. $CaCO_3$ is present in PMS as a filler in the papermaking process (Yoon et al., 2017). These peaks assigned to $CaCO_3$ were hardly found in PMSB800, which could be attributed to the decomposition or crystallographic form transition of $CaCO_3$ at 800 °C. A weak peak at 2θ = 32.2° could be recognized as CaO (PDF#99–0070). Wang et al. (2021) also observed that the XRD peak of CaO was weak in a calcium-containing porous biochar adsorbent. The presence of Ca on the surface was also confirmed by the TEM-EDS data (Fig. 5). It is likely that the $CaCO_3$ decomposition product CaO was able to form a stable precipitate with P, which contributed to the significant enhancement of P removal by PMSB800. PMSB300 had typical peaks for Fe_2O_3 at 2θ = 30°, 35.1°, 43.7°, 58.8°, 63.3° (PDF#40–1139), which was transformed from the ferric salt in the PMS. When the pyrolysis temperature was increased to 500 °C, additional peaks were observed at 2θ = 30°, 35.2°, 43°, 57.2°, and 62.7°, which corresponded to Fe_3O_4 (PDF#01–1111) (Yoon et al., 2017). The formation of Fe_3O_4 was also responsible for the magnetic properties of PMSB500, which facilitated the separation of the PMSBs. The peaks of Fe_3O_4 disappeared at a pyrolysis temperature of 700 °C, and the new peaks at 2θ = 35.9°, 41.7°, 60.5°related to FeO (PDF#89–0687) were formed, indicating that a reduction of Fe_3O_4 occurred during pyrolysis. Furthermore, significant peaks were observed in PMSB800 at 2θ = 44.8° and 65.2°, corresponding to Fe^0. It can be concluded that the ferric salt in the PMS was oxidized to Fe_2O_3 at the initial temperature up to approximately 300 °C, and then was reduced to lower-valent iron species (Fe_3O_4, FeO, Fe^0) with further pyrolysis temperature increments from 500 to 800 °C. The pyrolysis of PMS in this study occurred in an O-limited environment with continuous N_2 purging, producing reductive substances, such as syngas, including CH_4, CO, and H_2 (Cho et al., 2017; Choi et al., 2020; Yoon et al., 2019b). These syngas may provide a reductive environment and be responsible for transforming Fe from an oxidized state to a reduced form. The nanoscale ZVI Fe^0 has excellent P removal efficiency (245.65 mg P/g) via adsorption and coprecipitation processes (Wen et al., 2014), which could explain the significantly higher P removal by PMSB800 in this study.

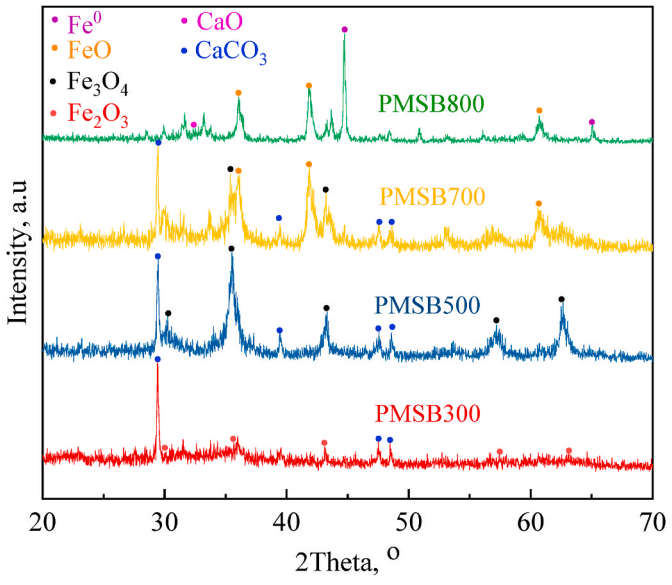

Fig. 6. XRD patterns of PMSBs.

3.2.3. XPS spectra of paper mill sludge biochars

To further elucidate the phosphate adsorption mechanisms of the PMSBs, PMSB800 (the best performing PMSB in this study) was analyzed by XPS before and after phosphate adsorption (Fig. 7). Compared with the pristine PMSB800 before adsorption (Fig. 7a), a new peak corresponding to P 2p was observed in the wide-scan survey spectra of the used PMSB800, indicating successful phosphate loading onto this biochar (Ren et al., 2016). This result was confirmed via high-resolution XPS, where the spectra clearly show the presence of a P 2p peak after P adsorption (Fig. 7b). In the reacted PMSB800, the new peak at 133.5 eV can be assigned to the adsorbed P, implying the formation of a Fe phosphate complex (such as $FePO_4$) on the PMSB800 surface (Li et al., 2019; Sleiman et al., 2016). This is consistent with previously reported results (Mallet et al., 2013). Fig. 7c and d shows the high-resolution spectra of the O 1s of the PMSBs before and after P adsorption, and three types of surface oxygen species could be identified. The peaks at the binding energies of ~529.9, ~531.5, and ~532.8 eV can be attributed to oxide-oxygen (O^{2-}, i.e., Fe–O or Ca–O), a hydroxyl group (–OH, i.e., Fe–OH or P–OH), and adsorbed water (H_2O), respectively (Yu et al., 2020; Yu et al., 2019). Wang et al. (2021) suggested that the XPS peak at the binding energy of 529.9 eV was believed to be the O 1s in CaO, which was consistent with the hypothesis of this study. CaO was produced by the decomposition of $CaCO_3$ in paper mill sludge. After the adsorption of P, the percentage of Fe–O decreased from 33.9% to 18.8%, while that of –OH increased from 54.6% to 62.5%, which is consistent with the results reported by Zhang et al. (2020b) and Wan et al. (2020). The increase in

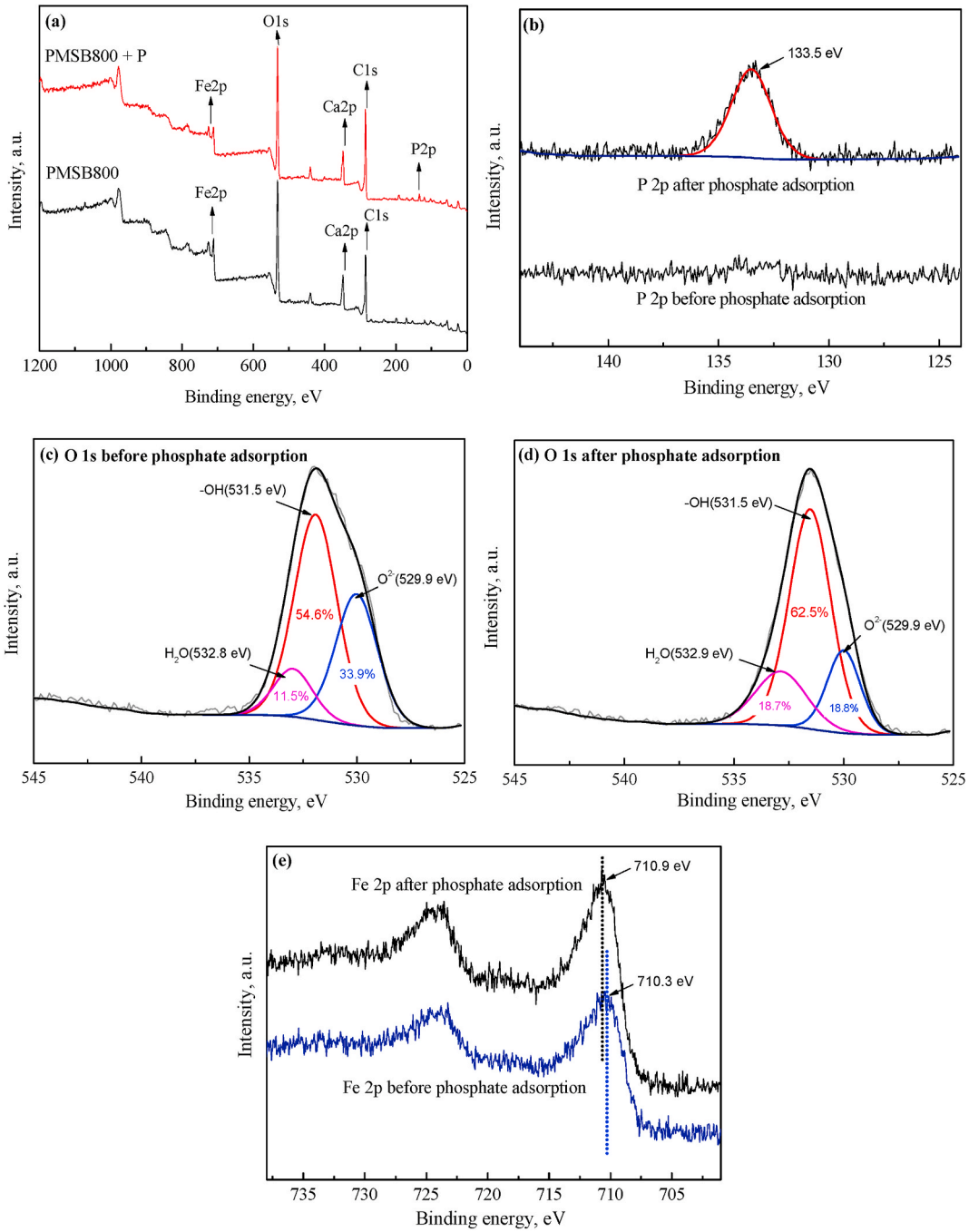

Fig. 7. High-resolution XPS spectra of PMSB800 before and after P adsorption.
(a) Wide survey XPS spectra, (b) P 2p, (c, d) O 1s, and (e) Fe 2p.

–OH after P adsorption was believed to represent both –OH and P–O bonding to form Fe–O–P ternary complexation via ligand exchange on the PMSB800 surface (Wan et al., 2020; Zhang et al., 2020b), which promoted P removal. This specific adsorption can be described by the equation presented below (Eq. (5)).

$$PMSB = Fe - OH + H_xPO_4^{(3-x)-} + H^+ \leftrightarrow \equiv Fe - PO_4 + H_2O \quad (5)$$

Furthermore, after phosphate adsorption, the Fe 2p band (Fig. 7e) in the phosphate-loaded PMSB800 was quite similar to that of the fresh PMSB800, indicating that Fe was still present on the surface of PMSB800 even after adsorption (Doliente et al., 2017). However, the Fe $2p_{2/3}$ shifted from 710.3 to 710.9 eV, suggesting that ≡Fe–OH from PMSB800 can contribute to phosphate sequestration by generating different oxidation states of Fe–PO_4 complexation (Zhang et al., 2016).

Summing up the above discussion, the two most likely mechanisms of P removal using PMSB800 are as follows. First, ferric oxides, such as FeO, the conversion of Fe^0 to iron corrosion products, removed P by coprecipitation and adsorption (Wan et al., 2020). Second, the inner-sphere complexation played a dominant role, via ligand exchange, during the phosphate removal by forming Fe–O–P ternary complexes, such as Fe–PO_4. These conclusions are in accord with the findings by Wen et al. (2014) that coprecipitation is one of the main mechanisms for the P by nanoscale zero-valent-iron.

4. Conclusions

In this study, PMSBs were obtained via one-step pyrolysis of waste PMS, and the potential for P removal from water was evaluated and characterized. PMS waste can be transformed into an effective adsorbent for P removal, with the highest temperature biochar PMSB800 having the greatest Q_m for P. The reductive pyrolysis atmosphere transformed the ferric salt in the sludge into ferric oxide and Fe^0 in the PMSBs, which facilitated the adsorption of P. The presence of Fe^0 in PMSB800 played a significant role in the enhancement of P removal via adsorption and coprecipitation by providing complexation sites for P to form Fe–O–P ternary complexes. Furthermore, the CaO in PMSB800 (decomposed from $CaCO_3$ at 800 °C) may also contribute to the significant enhancement of Q_m. The adsorption of P by PMSB800 is a spontaneous and endothermic process, meaning that an increase in ambient temperature promotes P adsorption. Moreover, the formation of Fe oxide and Fe^0 facilitated the magnetic separation of PMSB from water/wastewater. In conclusion, PMSB is a metal/metal oxide-embedded biochar with excellent P removal capability, with potential for simple magnetic separation, which is easily obtained from PMS waste via a one-step pyrolysis process.

Credit author statement

Ming Zhang: Conceptualization, Data curation, Formal analysis, Investigation, Methodology, Validation, Visualization, Writing – original draft, Writing – review & editing. Kun Lin: Formal analysis, Investigation, Visualization, Writing – original draft. Xiaodian Li: Formal analysis, Validation, Writing – review & editing. Lijun Wu: Formal analysis, Validation, Writing – review & editing. Jie Yu: Formal analysis, Validation, Writing – review & editing. Shuang Cao: Formal analysis, Validation, Writing – review & editing. Dong Zhang: Writing – review & editing. Liheng Xu: Writing – review & editing. Sanjai J. Parikh: Conceptualization, Writing – review & editing. Yong Sik Ok: Conceptualization, Funding acquisition, Methodology, Project administration, Resources, Supervision, Writing – original draft, Writing – review & editing.

Declaration of competing interest

The authors declare that they have no known competing financial interests or personal relationships that could have appeared to influence the work reported in this paper.

Acknowledgment

This research was financially supported by the Natural Science Foundation of Zhejiang Province (Grant No. HZ22E083129).

Appendix A. Supplementary data

Supplementary data to this article can be found online at https://doi.org/10.1016/j.envpol.2021.118521.

References

Ahmad, M., Rajapaksha, A.U., Lim, J.E., Zhang, M., Bolan, N., Mohan, D., Vithanage, M., Lee, S.S., Ok, Y.S., 2014. Biochar as a sorbent for contaminant management in soil and water: a review. Chemosphere 99, 19–33.
Chandra, S., Medha, I., Bhattacharya, J., 2020. Potassium-iron rice straw biochar composite for sorption of nitrate, phosphate, and ammonium ions in soil for timely and controlled release. Sci. Total Environ. 712.
Chintala, R., Mollinedo, J., Schumacher, T.E., Papiernik, S.K., Malo, D.D., Clay, D.E., Kumar, S., Gulbrandson, D.W., 2013. Nitrate sorption and desorption in biochars from fast pyrolysis. Microporous Mesoporous Mater. 179, 250–257.
Cho, D.W., Kwon, G., Yoon, K., Tsang, Y.F., Ok, Y.S., Kwon, E.E., Song, H., 2017. Simultaneous production of syngas and magnetic biochar via pyrolysis of paper mill sludge using CO2 as reaction medium. Energy Convers. Manag. 145, 1–9.
Cho, D.W., Yoon, K., Ahn, Y., Su, Y.Q., Tsang, D.C.W., Hou, D.Y., Ok, Y.S., Son, H., 2019. Fabrication and environmental applications of multifunctional mixed metal-biochar composites (MMBC) from red mud and lignin wastes. J. Hazard Mater. 374, 412–419.
Choi, D., Jung, S.Y., Jeon, Y.J., Moon, D.H., Kwon, E.E., 2020. Study on carbon rearrangements of CO2 co-feeding pyrolysis of corn stover and oak wood. J Co2 Util 42.
Conley, D.J., Paerl, H.W., Howarth, R.W., Boesch, D.F., Seitzinger, S.P., Havens, K.E., Lancelot, C., Likens, G.E., 2009. ECOLOGY controlling eutrophication: nitrogen and phosphorus. Science 323 (5917), 1014–1015.
Cui, X.Q., Hao, H.L., He, Z.L., Stoffella, P.J., Yang, X.E., 2016. Pyrolysis of wetland biomass waste: potential for carbon sequestration and water remediation. J. Environ. Manag. 173, 95–104.
Doliente, J.E., Kim, Y., Nam, H., Choi, Y., 2017. Mill scale-derived magnetite particles: effective adsorbent for the removal of phosphate in aqueous solutions. J. Environ. Eng. 143 (12).
Fang, C., Zhang, T., Li, P., Jiang, R.F., Wang, Y.C., 2014. Application of magnesium modified corn biochar for phosphorus removal and recovery from swine wastewater. Int. J. Environ. Res. Publ. Health 11 (9), 9217–9237.
Freundlich, H.M.F., 1906. Over the adsorption in solution. J. Phys. Chem. 57, 385–471.
Gong, Y.P., Ni, Z.Y., Xiong, Z.Z., Cheng, L.H., Xu, X.H., 2017a. Phosphate and ammonium adsorption of the modified biochar based on Phragmites australis after phytoremediation. Environ. Sci. Pollut. Res. 24 (9), 8326–8335.
Gong, Y.P., Ni, Z.Y., Xiong, Z.Z., Cheng, L.H., Xu, X.H., 2017b. Phosphate and ammonium adsorption of the modified biochar based on Phragmites australis after phytoremediation. Environ. Sci. Pollut. Res. 24 (9), 8326–8335.
Hale, S.E., Alling, V., Martinsen, V., Mulder, J., Breedveld, G.D., Cornelissen, G., 2013. The sorption and desorption of phosphate-P, ammonium-N and nitrate-N in cacao shell and corn cob biochars. Chemosphere 91 (11), 1612–1619.
Ho, Y.S., 1995. Adsorption of Heavy Metals from Waste Streams by Peat. University of Birmingham, Birmingham.
Ho, Y.S., McKay, G., 1999. Pseudo-second order model for sorption processes. Process Biochem. 34 (5), 451–465.
Jung, K.W., Hwang, M.J., Ahn, K.H., Ok, Y.S., 2015. Kinetic study on phosphate removal from aqueous solution by biochar derived from peanut shell as renewable adsorptive media. Int J Environ Sci Te 12 (10), 3363–3372.
Kilic, M., Kirbiyik, C., Cepeliogullar, O., Putun, A.E., 2013. Adsorption of heavy metal ions from aqueous solutions by bio-char, a by-product of pyrolysis. Appl. Surf. Sci. 283, 856–862.
Lagergren, S., 1898. About the theory of so-called adsorption of soluble substances. K. - Sven. Vetenskapsakademiens Handl. 24, 1–39.
Langmuir, I., 1918. The adsorption of gases on plane surfaces of glass, mica and platinum. J. Am. Chem. Soc. 40, 1361–1403.
Li, Y.Y., Fu, F.L., Cai, W.T., Tang, B., 2019. Synergistic effect of mesoporous feroxyhyte nanoparticles and Fe(II) on phosphate immobilization: adsorption and chemical precipitation. Powder Technol. 345, 786–795.
Mallet, M., Barthelemy, K., Ruby, C., Renard, A., Naille, S., 2013. Investigation of phosphate adsorption onto ferrihydrite by X-ray Photoelectron Spectroscopy. J. Colloid Interface Sci. 407, 95–101.
Marschner, H., Marschner, P., 2012. Marschner's Mineral Nutrition of Higher Plants. Elsevier/Academic Press, London ; Waltham, MA.
Nielsen, P.H., McIlroy, S.J., Albertsen, M., Nierychlo, M., 2019. Re-evaluating the microbiology of the enhanced biological phosphorus removal process. Curr. Opin. Biotechnol. 57, 111–118.

Novais, S.V., Zenero, M.D.O., Barreto, M.S.C., Montes, C.R., Cerri, C.E.P., 2018a. Phosphorus removal from eutrophic water using modified biochar. Sci. Total Environ. 633, 825–835.
Novais, S.V., Zenero, M.D.O., Tronto, J., Conz, R.F., Cerri, C.E.P., 2018b. Poultry manure and sugarcane straw biochars modified with MgCl2 for phosphorus adsorption. J. Environ. Manag. 214, 36–44.
Oehmen, A., Lemos, P.C., Carvalho, G., Yuan, Z.G., Keller, J., Blackall, L.L., Reis, M.A.M., 2007. Advances in enhanced biological phosphorus removal: from micro to macro scale. Water Res. 41 (11), 2271–2300.
Park, J.H., Ok, Y.S., Kim, S.H., Cho, J.S., Heo, J.S., Delaune, R.D., Seo, D.C., 2015. Evaluation of phosphorus adsorption capacity of sesame straw biochar on aqueous solution: influence of activation methods and pyrolysis temperatures. Environ Geochem Hlth 37 (6), 969–983.
Ren, Z.F., Xu, X., Wang, X., Gao, B.Y., Yue, Q.Y., Song, W., Zhang, L., Wang, H.T., 2016. FTIR, Raman, and XPS analysis during phosphate, nitrate and Cr(VI) removal by amine cross-linking biosorbent. J. Colloid Interface Sci. 468, 313–323.
Ruan, Z.H., Wu, J.H., Huang, J.F., Lin, Z.T., Li, Y.F., Liu, Y.L., Cao, P.Y., Fang, Y.P., Xie, J., Jiang, G.B., 2015. Facile preparation of rosin-based biochar coated bentonite for supporting alpha-Fe2O3 nanoparticles and its application for Cr(VI) adsorption. J. Mater. Chem. 3 (8), 4595–4603.
Schindler, D.W., 1974. Eutrophication and recovery in experimental lakes - implications for lake management. Science 184 (4139), 897–899.
Sleiman, N., Deluchat, V., Wazne, M., Mallet, M., Courtin-Nomade, A., Kazpard, V., Baudu, M., 2016. Phosphate removal from aqueous solution using ZVI/sand bed reactor: behavior and mechanism. Water Res. 99, 56–65.
Wan, J., Wu, B.L., Lo, I.M.C., 2020. Development of Fe^0/Fe_3O_4 composites with tunable properties facilitated by Fe^{2+} for phosphate removal from river water. Chem. Eng. J. 388, 124242.
Wang, Z., Miao, R., Ning, P., He, L., Guan, Q., 2021. From wastes to functions: a paper mill sludge-based calcium-containing porous biochar adsorbent for phosphorus removal. J. Colloid Interface Sci. 593, 434–446.
Wang, Z.H., Guo, H.Y., Shen, F., Yang, G., Zhang, Y.Z., Zeng, Y.M., Wang, L.L., Xiao, H., Deng, S.H., 2015. Biochar produced from oak sawdust by Lanthanum (La)-involved pyrolysis for adsorption of ammonium (NH4+), nitrate (NO3-), and phosphate (PO43-). Chemosphere 119, 646–653.
Wang, Z.H., Shen, D.K., Shen, F., Li, T.Y., 2016. Phosphate adsorption on lanthanum loaded biochar. Chemosphere 150, 1–7.
Wang, Z.Y., Bakshi, S., Li, C.Y., Parikh, S.J., Hsieh, H.S., Pignatello, J.J., 2020. Modification of pyrogenic carbons for phosphate sorption through binding of a cationic polymer. J. Colloid Interface Sci. 579, 258–268.
Wen, Z.P., Zhang, Y.L., Dai, C.M., 2014. Removal of phosphate from aqueous solution using nanoscale zerovalent iron (nZVI). Colloid. Surface. 457, 433–440.
Xia, Y.F., Zhang, M., Tsang, D.C.W., Geng, N., Lu, D.B., Zhu, L.F., Igalavithana, A.D., Dissanayake, P.D., Rinklebe, J., Yang, X., Ok, Y.S., 2020. Recent advances in control technologies for non-point source pollution with nitrogen and phosphorous from agricultural runoff: current practices and future prospects. Appl Biol Chem 63 (1).
Yao, Y., Gao, B., Chen, J., Zhang, M., Inyang, M., Li, Y., Alva, A., Yang, L., 2013a. Engineered carbon (biochar) prepared by direct pyrolysis of Mg-accumulated tomato tissues: characterization and phosphate removal potential. Bioresour. Technol. 138, 8–13.
Yao, Y., Gao, B., Chen, J.J., Yang, L.Y., 2013b. Engineered biochar reclaiming phosphate from aqueous solutions: mechanisms and potential application as a slow-release fertilizer. Environ. Sci. Technol. 47 (15), 8700–8708.
Ye, Y.Y., Ngo, H.H., Guo, W.S., Liu, Y.W., Li, J.X., Liu, Y., Zhang, X.B., Jia, H., 2017. Insight into chemical phosphate recovery from municipal wastewater. Sci. Total Environ. 576, 159–171.
Yin, Q.Q., Wang, R.K., Zhao, Z.H., 2018. Application of Mg-Al-modified biochar for simultaneous removal of ammonium, nitrate, and phosphate from eutrophic water. J. Clean. Prod. 176, 230–240.
Yoon, K., Cho, D.W., Bhatnagar, A., Song, H., 2020. Adsorption of As(V) and Ni(II) by Fe-Biochar composite fabricated by co-pyrolysis of orange peel and red mud. Environ. Res. 188.
Yoon, K., Cho, D.W., Tsang, D.C.W., Bolan, N., Rinklebe, J., Song, H., 2017. Fabrication of engineered biochar from paper mill sludge and its application into removal of arsenic and cadmium in acidic water. Bioresour. Technol. 246, 69–75.
Yoon, K., Jung, J.M., Cho, D.W., Tsang, D.C.W., Kwon, E.E., Song, H., 2019a. Engineered biochar composite fabricated from red mud and lipid waste an synthesis of biodiesel using the composite. J. Hazard Mater. 366, 293–300.
Yoon, K., Lee, S.S., Ok, Y.S., Kwon, E.E., Song, H., 2019b. Enhancement of syngas for H-2 production via catalytic pyrolysis of orange peel using CO2 and bauxite residue. Appl. Energy 254.
Yu, J., Zeng, T., Wang, H., Zhang, H., Sun, Y.P., Chen, L., Song, S., Li, L.X.Y., Shi, H.X., 2020. Oxygen-defective MnO_2-x rattle-type microspheres mediated singlet oxygen oxidation of organics by peroxymonosulfate activation. Chem. Eng. J. 394.
Yu, J., Zhang, J., Zeng, T., Wang, H., Sun, Y.P., Chen, L., Song, S., Shi, H.X., 2019. Stable incorporation of MnOx quantum dots into N-doped hollow carbon: a synergistic peroxymonosulfate activator for enhanced removal of bisphenol A. Separ. Purif. Technol. 213, 264–275.
Zeng, Z., Zhang, S.D., Li, T.Q., Zhao, F.L., He, Z.L., Zhao, H.P., Yang, X.E., Wang, H.L., Zhao, J., Rafiq, M.T., 2013a. Sorption of ammonium and phosphate from aqueous solution by biochar derived from phytoremediation plants. J. Zhejiang Univ. - Sci. B 14 (12), 1152–1161.
Zeng, Z., Zhang, S.D., Li, T.Q., Zhao, F.L., He, Z.L., Zhao, H.P., Yang, X.E., Wang, H.L., Zhao, J., Rafiq, M.T., 2013b. Sorption of ammonium and phosphate from aqueous solution by biochar derived from phytoremediation plants. J. Zhejiang Univ. - Sci. B 14 (12), 1152–1161.
Zhang, F., Xu, D.P., Wang, Y.G., Argyle, M.D., Fan, M.H., 2015. CO2 gasification of Powder River Basin coal catalyzed by a cost-effective and environmentally friendly iron catalyst. Appl. Energy 145, 295–305.
Zhang, M., Ahmad, M., Lee, S.S., Xu, L.H., Ok, Y.S., 2014. Sorption of polycyclic aromatic hydrocarbons (PAHs) to lignin: effects of hydrophobicity and temperature. Bull. Environ. Contam. Toxicol. 93 (1), 84–88.
Zhang, M., Gao, B., Yao, Y., Xue, Y.W., Inyang, M., 2012. Synthesis of porous MgO-biochar nanocomposites for removal of phosphate and nitrate from aqueous solutions. Chem. Eng. J. 210, 26–32.
Zhang, M., Song, G., Gelardi, D.L., Huang, L.B., Khan, E., Masek, O., Parikh, S.J., Ok, Y.S., 2020a. Evaluating biochar and its modifications for the removal of ammonium, nitrate, and phosphate in water. Water Res. 186.
Zhang, Q.R., Teng, J., Zou, G.D., Peng, Q.M., Du, Q., Jiao, T.F., Xiang, J.Y., 2016. Efficient phosphate sequestration for water purification by unique sandwich-like MXene/magnetic iron oxide nanocomposites. Nanoscale 8 (13), 7085–7093.
Zhang, Z.R., Yu, H.Q., Zhu, R.X., Zhan, X., Yan, L.G., 2020b. Phosphate adsorption performance and mechanisms by nanoporous biochar-iron oxides from aqueous solutions. Environ. Sci. Pollut. Res. 27, 28132–28145.
Zhou, L., Xu, D.F., Li, Y.X., Pan, Q.C., Wang, J.J., Xue, L.H., Howard, A., 2019. Phosphorus and nitrogen adsorption capacities of biochars derived from feedstocks at different pyrolysis temperatures. Water-Sui 11 (8), 1559.
Zhu, R.L., Zhu, L.Z., 2008. Thermodynamics of naphthalene sorption to organoclays: role of surfactant packing density. J. Colloid Interface Sci. 322 (1), 27–32.